Journal of Magnetism and Magnetic Materials 364 (2014) 24–33

Contents lists available at ScienceDirect

Journal of Magnetism and Magnetic Materials

journal homepage: www.elsevier.com/locate/jmmm

Thermomagnetic behaviour and compositional irreversibility on $(Fe/Si)_3$ multilayer films

L. Badía-Romano [a,b,*], J. Rubín [a,c], C. Magén [b,d,e], F. Bartolomé [a,b], J. Sesé [b,d], M.R. Ibarra [b,d], J. Bartolomé [a,b], A. Hierro-Rodriguez [f], J.I. Martín [g,h], J.M. Alameda [g,h], D.E. Bürgler [i], S.N. Varnakov [j,k], S.V. Komogortsev [j,k], S.G. Ovchinnikov [j,l]

[a] Instituto de Ciencia de Materiales de Aragón, CSIC-Universidad de Zaragoza, E-50009 Zaragoza, Spain
[b] Departamento de Física de la Materia Condensada, Universidad de Zaragoza, E-50009 Zaragoza, Spain
[c] Departamento de Ciencia de Materiales e Ingeniería Metalúrgica, Universidad de Zaragoza, E-50018 Zaragoza, Spain
[d] Laboratorio de Microscopías Avanzadas (LMA), Instituto de Nanociencia de Aragón (INA), Universidad de Zaragoza, E-50018 Zaragoza, Spain
[e] Fundación ARAID, E-50004 Zaragoza, Spain
[f] IN-IFIMUP, Departamento de Física e Astronomia, Faculdade de Ciências, Universidade do Porto, Rua Campo Alegre 687, 4169-007 Porto, Portugal
[g] Departamento de Física, Universidad de Oviedo, E-33007 Oviedo, Spain
[h] CINN (CSIC-Universidad de Oviedo-Principado de Asturias), E-33007 Oviedo, Spain
[i] Peter Grünberg Institute (PGI-6), Electronic Properties, Forschungszentrum Jülich GmbH, D-52425 Jülich, Germany
[j] Kirensky Institute of Physics, Siberian Division, Russian Academy of Sciences, Akademgorodok, Krasnoyarsk, 660036 Russia
[k] Siberian Aerospace University, pr. im. gazety "Krasnoyarskii rabochii" 31, Krasnoyarsk 660014 Russia
[l] Siberian Federal University, 79 Svobodny Prospect, Krasnoyarsk, 660036 Russia

ARTICLE INFO

Article history:
Received 12 December 2013
Received in revised form
4 April 2014
Available online 15 April 2014

Keywords:
Fe–Si multilayer
Chemical transformation
Fe silicide
Interlayer exchange coupling
Magnetic domain
in situ annealing

ABSTRACT

This work presents the correlation between the morphology and magnetic properties of $(Fe/Si)_3$ multilayers with different Fe layer thicknesses and fixed Si spacer thickness in a broad temperature range ($5 < T < 800$ K). Films were prepared by thermal evaporation under ultrahigh vacuum onto a buffer layer of Fe/Ag deposited on a GaAs(001) substrate. Transmission electron microscopy reveals good epitaxial growth and phase transformations in the c-FeSi phase formed during deposition as well as upon subsequent annealing of the sample up to 800 K. Remanence to saturation magnetization M_R/M_S ratios and saturation fields are related to several types of interlayer exchange coupling. 90°-coupling and a superposition of 90° and antiferromagnetic interlayer exchange coupling are found depending on the Fe layer thickness. Magnetization curves were investigated as a function of temperature by *in situ* annealing. They show an irreversible thermal process as temperature increases from 300 to 450 K that is correlated to the formation of a ferromagnetic silicide phase. At higher temperature this phase transforms into a paramagnetic Fe–Si phase.

1. Introduction

The research field on nanostructures of ferromagnetic metal/semiconductor materials is subject of interest due to their unique physical properties for applications in microelectronics, spintronics, etc. [1–9]. The possibility of spin polarized injection of carriers from a ferromagnetic layer to a semiconducting one may be used in the generation of spintronic devices which can show additional functionalities [10], increased data processing speed, lower power consumption, and increased device density in chip integrated circuits [11]. The Fe–Si system is a representative candidate for studying the use of ferromagnet/semiconductor heterostructures for device technologies. This system has various stoichiometric phases such as the semiconducting β-$FeSi_2$ [12,13], amorphous [14] and nanocrystalline-$FeSi_2$ [15,16], paramagnetic ϵ-FeSi [17], ferromagnetic Fe_3Si [18–21] and epitaxially stable c-FeSi with the CsCl structure [21–26]. Additionally, weak ferromagnetism has been recently reported in ϵ-FeSi thin films [27]. On the other hand, the interlayer exchange coupling (IEC) between two ferromagnetic layers across a nonmagnetic spacer, together with the giant magnetoresistence [1,28], leads to several technological applications in mass storage, nonvolatile memory [29], and sensors. $(Fe/Si)_n$ multilayers have been one of the model systems since it is quite compatible with Si microchip technology. However, the possible presence of non-magnetic silicides decreases the

* Corresponding author. Tel.:+34 976761218; fax:+34 976761218.
E-mail address: lbadia@unizar.es (L. Badía-Romano).

http://dx.doi.org/10.1016/j.jmmm.2014.04.029
0304-8853/

current spin polarization in the silicon spacer layer and affects the IEC mechanism. It is, therefore, of utmost importance to assess the interlayer composition.

We briefly review the antecedents known on the IEC in the Fe/Si multilayer system. It has been studied under different conditions of substrate and substrate temperature [24], composition and thickness of the non-magnetic spacer [22,23,30–33], temperature [23,24,32,33] or number of Fe/Si bilayers [34,24]. These works show an oscillatory [8] or exponential decay [25] of coupling versus the spacer layer thickness depending on the composition and structure of the spacer layer. Both types of thickness dependence, oscillatory and exponential, are explained by the quantum interference multilayer model [35], which predicts oscillations in the bilinear exchange coupling constant for semiconductor and metallic spacers, while insulating spacers are expected to show an exponential decay with the spacer thickness. The strongest antiferromagnetic (AF) coupling of up to 8 erg/cm^2 [36,37] was found for samples prepared according to the growth procedure employed in the present work. These samples exhibited an exponential spacer thickness dependence of IEC. Only a few works have studied the dependence of IEC on the number of (Fe/Si) bilayers [34], but in all cases the number of bilayers was even, probably to avoid the signal of the uncompensated magnetic layer in the case of AF coupling. Throughout the extensive work on the thickness, composition and number of spacers, it has been concluded that the thickness of the magnetic layers seems to play no role for the character of the interlayer coupling.

In this work we focus on the particular case of $(Fe/Si)_n$ multilayer magnetic structures with a reduced and odd number of Fe layers and their interfaces. To understand their behaviour one needs to assess their dependence on the Fe film thickness, the constitution of the interlayer spacer, and the magnetic domain structure, while maintaining a nominally identical Si spacer thickness.

In a previous work the magnetization of $(Fe/Si)_3$ multilayers, grown by thermal evaporation in an ultrahigh vacuum system, was investigated at high temperature as a function of Fe layer thickness [38]. The nominal Si spacer was found to include Fe silicides. The fraction of nonmagnetic silicide phases was estimated versus the Fe layer thickness, for a series of (Fe/Si) trilayers deposited on naturally oxidized Si(100) and Si(111) substrates. It was also demonstrated that nonmagnetic silicide phases are formed during both the synthesis procedure and the subsequent annealing. It was concluded that the degree of silicide formation is strongly dependent on the crystalline quality of the multilayers and in particular on the interface roughness and structure. These samples kept their thermal stability up to a temperature of about 400 K.

The application of these multilayers in spintronic devices, which may be located in very extreme environments, confers great importance to establish their performance limits. The operational temperature of such devices may be limited by the evolution of the interface composition. Therefore, in this work we have explored the magnetization dependence on temperature. The relative amount of non-magnetic phases, which are formed both during the synthesis process of $(Fe/Si)_3$ films and due to processes of silicides formation at high temperatures, has been studied up to the destruction of the multilayer device.

We prepared a new series of samples consisting of sequentially deposited Fe/Si bilayers on an *in situ* prepared buffer layer of Fe/Ag on a GaAs(001) substrate, since this method has been reported to improve crystallinity and reduce roughness [39]. In order to compare with previous works we have chosen nominally identical Fe layer thickness values as in [38], in the range between 1.2 and 3.8 nm, and a fixed Si spacer thickness of 1.5 nm. Such Fe films are ferromagnetic, with their easy axis parallel to the substrate plane [40].

The paper is organized as follows: the experimental techniques and sample preparation details are given in Section 2. In Section 3 the microstructural characterization of the multilayers performed with high resolution transmission electron microscopy (HRTEM) and scanning transmission electron microscopy (STEM) combined with electron energy loss spectroscopy (EELS) is given for two selected samples. In Section 4 the experimental results from dc magnetization performed with a SQUID magnetometer from 5 K to 800 K are given. They allow to follow the evolution of the magnetic phases *in situ* as they are formed upon annealing. The results of the work are discussed in Section 5, and the conclusions are presented in Section 6.

2. Experimental details

Multilayers with the full layer sequence GaAs/Fe(1 nm)/Ag (150 nm)/Fe(d_{Fe})/Si(1.5 nm)/Fe(d_{Fe})/Si(1.5 nm)/Fe(d_{Fe})/Si(10 nm), where d_{Fe} is the nominal iron layer thickness, were prepared by thermal evaporation in a molecular-beam epitaxy system. First, a buffer layer of Fe (1 nm)/Ag (150 nm) was deposited on GaAs (001) substrate. On top, three repetitions of the bilayer Fe(d_{Fe})/Si (1.5 nm), with the last Si layer of 10 nm thickness as capping, were grown. The background pressure was better than 10^{-10} mbar. The thicknesses and the deposition rates, of about 0.6 nm/min for both Fe and Si, were controlled by a calibrated quartz crystal monitor, and the layers were characterized by Auger electron spectroscopy and low-energy electron diffraction (LEED). All Fe and Si layers were deposited at RT. The well-defined LEED pattern observed throughout the whole structure indicated a good epitaxial growth [41].

Since the samples' buffers contain a magnetic layer, samples with substrate and buffer only, i.e., before multilayer deposition, were kept aside to determine independently their magnetic contribution. All the samples were cut into pieces of 2 mm × 5 mm in size. In these samples the easy axes of magnetization are at an angle of 45° to the edges of the rectangular GaAs substrate. The investigated films have varying d_{Fe} (sample A: $d_{Fe} = 1.2$ nm, B: $d_{Fe} = 1.6$ nm, C: $d_{Fe} = 2.6$ nm and D: $d_{Fe} = 3.8$ nm). The samples were designated by the subscript "m" to refer to complete sample, i.e., substrate, buffer and the $(Fe/Si)_3$ multilayer (sample X_m), and by the subscript "n" to refer to the sample with only substrate and buffer (sample X_n), see Fig. 1.

HRTEM images were obtained in a FEI Titan Cube microscope equipped with an image aberration corrector and operated at 300 kV. High angle annular dark field (HAADF) STEM imaging combined with EELS was performed in a probe corrected FEI Titan TEM equipped with a Gatan Tridiem 866 ERS energy filter and operated at 300 kV. A probe size of about 0.2 nm was used in the STEM-EELS spectrum lines. The TEM specimens were cross sectional lamellae of about 50 nm thickness fabricated in a FEI Helios

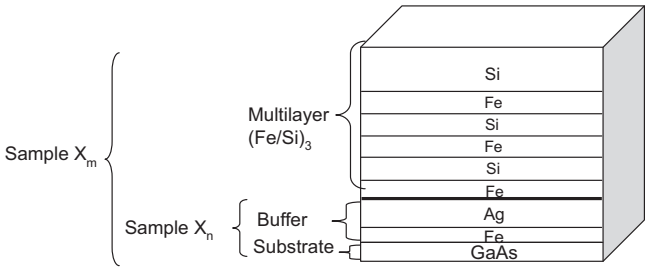

Fig. 1. Scheme of the multilayer samples. X= A($d_{Fe} = 1.2$ nm), B($d_{Fe} = 1.6$ nm), C ($d_{Fe} = 2.6$ nm), and D($d_{Fe} = 3.8$ nm). The Si top layer and the Fe and Ag buffer layers thicknesses are the same for all the samples ($d_{Si} = 1.5$ nm, $d_{Si\ top\ layer} = 10$ nm, $d_{Ag} = 150$ nm and $d_{FeBuffer} = 1$ nm).

600 Nanolab. The single crystal substrate zone axis of the lamella was used to orient it to insure that the interfaces were perpendicular to the image plane, i.e., parallel to the direction of the electron beam.

Magnetic domains were observed using the longitudinal magneto-optical Kerr effect (L-MOKE) with a Xe lamp emitting white light. The sample was mounted on a 0–360° rotating stage with 1° precision. In-plane magnetic fields up to 1 kOe were applied parallel to the incidence direction of the light. Field dependent imaging of the domains at RT was obtained along an hysteresis curve.

The magnetic measurements were carried out using a MPMS SQUID magnetometer from Quantum Design with applied fields up to 50 kOe. The magnetization in the temperature range from 5 to 300 K was measured with the reciprocating sample option (RSO), and a standard plastic straw sample holder, while for the 300–800 K range the oven option was used with the sample holder consisting of a twisted thin aluminium foil sheet where the sample was located in the middle of the resulting rod [3]. The sample was held in a helium atmosphere of 2 mbar pressure that allowed a clean annealing, and *in situ* magnetization measurements during the annealing. Since the sample showed planar magnetic anisotropy, as expected for Fe thin films, the magnetization was measured with the applied field parallel to the film plane in all cases to avoid demagnetization factor correction. The magnetization hysteresis loops were measured at different fixed temperatures for the samples X_m and X_n along the Fe[110] direction. The magnetic contribution of the $(Fe/Si)_3$ multilayer was obtained by subtraction $M_X = M_{X_m} - M_{X_n}$, which eliminates the substrate contribution, including the Fe buffer layer and the diamagnetic contribution mostly produced by the GaAs substrate, since that of the 150 nm Ag layer is negligible. The magnetization versus temperature measurements $M(T)$ on samples X_n and X_m were carried out in an external field $H=1$ kOe. Annealing was carried out at a rate of 5 K/min. The total magnetization at each temperature range was corrected by the substrate contribution. The $M(T)$ data in the 300–800 K range were scaled to match the $M(T)$ data between 5 and 350 K (RSO) in the common temperature range, 300–350 K, since the low temperature SQUID data are measured with a higher accuracy.

3. Microstructure characterization

3.1. Pristine sample D

The HRTEM image of the pristine sample D (maximum Fe thickness d_{Fe}) displayed in Fig. 2(a) shows good crystallinity and epitaxial growth of the stack on top of the Ag buffer and a clear alternation of the Fe and Si layers. Fig. 2(b) depicts the Fast Fourier Transform (FFT) of the image, which represents a digital diffractogram containing reflections or spots corresponding to the crystal periodicities. Note the absence of a set of reflections matching those of crystalline silicon and the presence of some reflections consistent with the silicide c-FeSi with CsCl structure (space group Pm3m) and lattice parameter $a=2.77$ Å [6].

HAADF-STEM imaging (Fig. 3, left) shows the multilayer $(Fe/Si)_3$ as in the HRTEM image. The HAADF intensity profile perpendicular to the interfaces extracted from Fig. 3 (Fig. 4(a)) shows three oscillations with the same shape and height, which correspond to the three Fe layers of the sample. The estimated thickness of each Fe layer (width of the plateau at the top of each

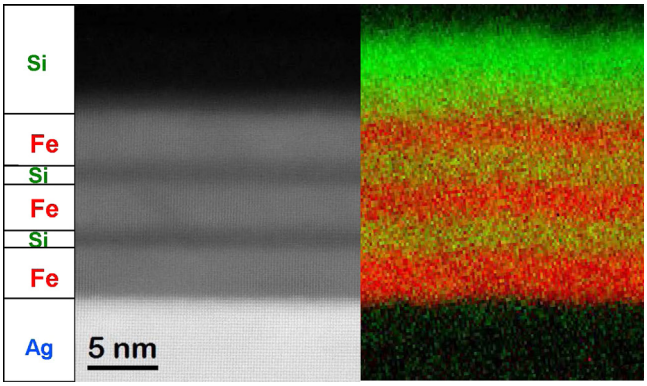

Fig. 3. (Left) HAADF-STEM-image of the pristine sample D. Left column indicates the nominal trilayer structure. (Right) Chemical map from the STEM-EELS spectrum imaging experiment. Red: Fe M-edge, green: Si L-edge. (For interpretation of the references to colour in this figure caption, the reader is referred to the web version of this paper.)

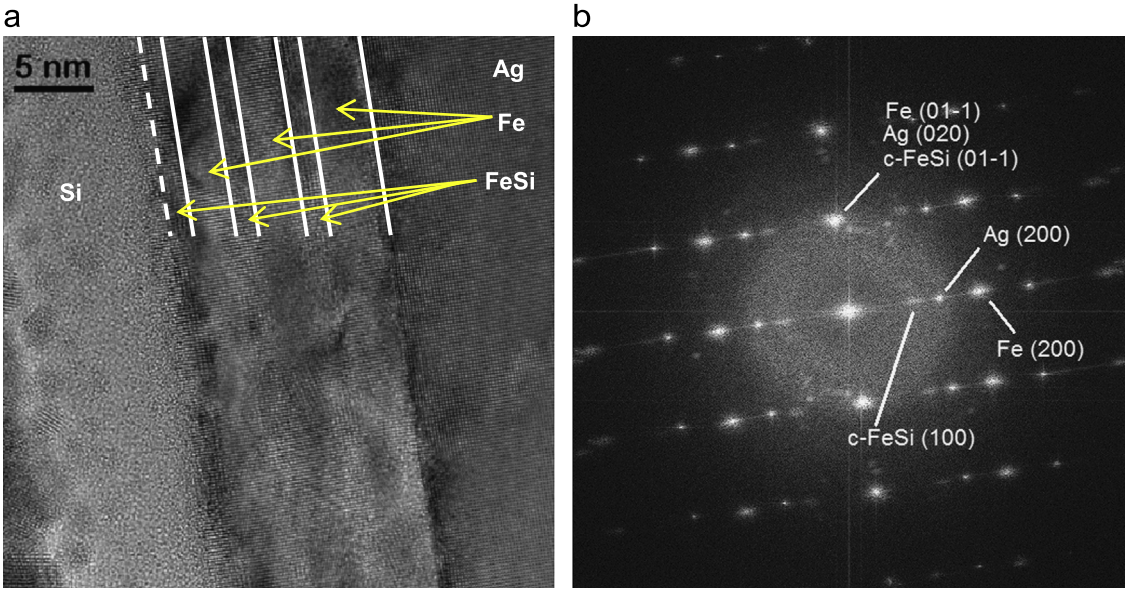

Fig. 2. Pristine sample D: (a) HRTEM image of the $(Fe/Si)_3$ multilayer grown on top of a Ag buffer. Full white lines indicate the nominal multilayer structure. The dashed line indicates the Fe–Si interface formed by FeSi. (b) FFT of the image. The main periodicities have been indexed according to existing materials (bulk Fe-, Ag- and silicon-containing materials).

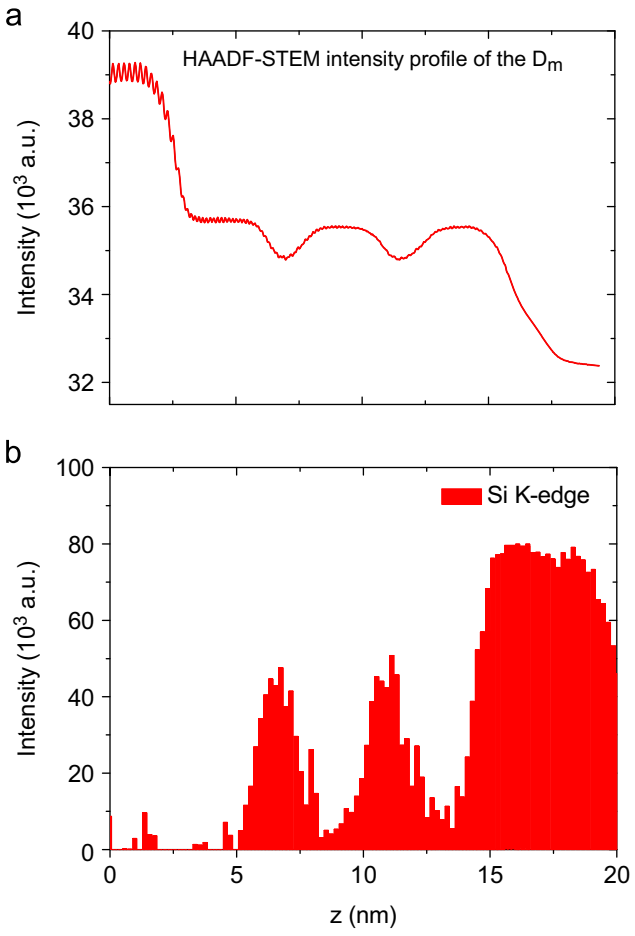

Fig. 4. (a) HAADF-STEM intensity profile of the pristine sample D perpendicular to the growth direction. (b) EELS intensity profile of the Si-K edge of the pristine sample D.

oscillation, which accounts for the Fe-richest region in the layers) is in agreement with the nominal thickness (3.8 nm) within an error of ± 0.6 nm.

A map of the integrated intensities of the Fe-M (54 eV) (red) and the Si-L (99 eV) (green) edges was obtained from a STEM-EELS spectrum imaging experiment (Fig. 3, right). From a qualitative point of view, there is a significantly large Fe signal in the Si layers, whereas there is hardly any Si signal in the Fe layers. The presence of Fe signal in the Si layers cannot be explained in terms of beam spread, dechanneling or delocalization of inelastic scattering. Actually, a further proof of the Fe presence in the Si layer is given by acquiring a STEM-EELS line profile to map the Si-K (1839 eV) edge signal (Fig. 4(b)), where no other edge is perturbing the extraction of the Si signal. In this case, the same behaviour of the Si signal at the intermediate thin layers is observed. Furthermore, in the spacers between the Fe layers the Si content is about 60% of the thick, topmost and pure Si capping layer. This result is in good agreement with Fe–Si alloying within the Si spacers, and consistent with the 1:1 atomic ratio of the structure c-FeSi.

3.2. *Annealed sample D*

After annealing up to 800 K at a rate of 5 K/min, the STEM-EELS image (Fig. 5(a)) shows that the multilayer structure disappears. Under the protective Pt-carbon layer used in the sample preparation for STEM, there is a nonuniform layer with a heterogeneous mixture of all components. The Ag buffer layer contains embedded Fe–Si particles that have been formed by reaction and segregated during the annealing, as a consequence of the immiscibility between Ag and Fe phases at 800 K [42]. The shell of these Fe–Si particles is richer in Fe with respect to the core (Fig. 5(b)).

4. Magnetic properties

The hysteresis curves $M(H)$ at 5 K measured for the different samples are shown in Fig. 6. The samples A, B, and C (Fig. 6(a–c)) display symmetric hysteresis loops characteristic of a ferromagnetic system. However, the sample D (Fig. 6(d)) shows a square loop at low fields and then a monotonous increase in magnetization which saturates at much larger applied fields than in the other samples with lower Fe layer thickness, which indicates an AF contribution.

Samples B, C and D show a similar square hysteresis loop shape at low fields with onset of magnetization reversal at a negative field in the second quadrant and similar coercivity $H_c \approx 36$ Oe (experimentally determined magnetic quantities for samples A–D are compiled in Table 1). In contrast, in the sample A (with the thinnest d_{Fe}) the reversal takes place at zero field and the decreasing field branch after reversal ($H < H_c$) collapses with the increasing one at H_m, leading to an appreciable broadening in the loop (Fig. 6(a)). Additionally, two changes of slope at -110 Oe and -990 Oe can be observed, which may indicate a reminiscence of reversal of magnetization of single layers at different field values. Since the applied field is along a hard axis of the Fe layer, no clear jumps in the $M(H)$ curves are observed. The slope change is also present in the sample D, but with a narrower loop.

To understand the evolution of the hysteresis cycle, field dependent imaging of the domains at RT was obtained by L-MOKE on the C sample along the [100] easy magnetization axis in the field range ± 1 kOe (Fig. 7). After saturation in the positive

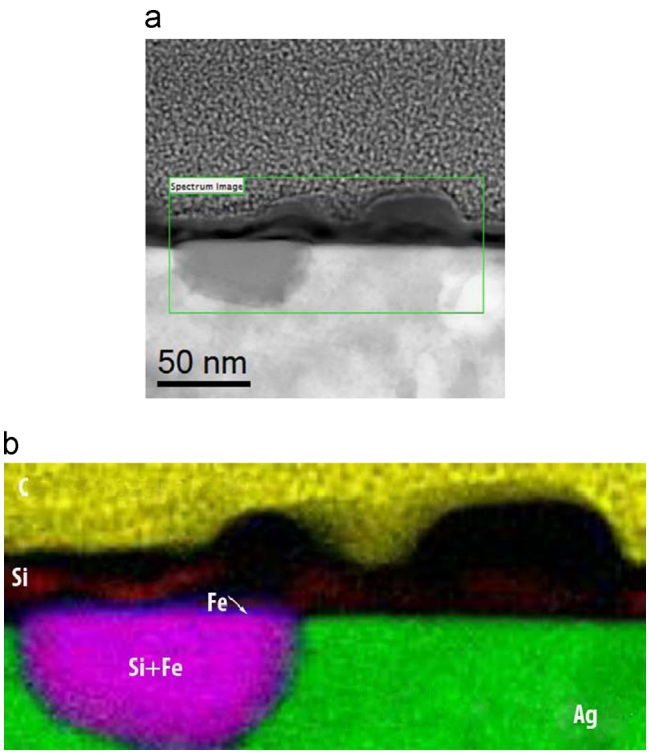

Fig. 5. (a) STEM-EELS image of the D multilayer $(Fe/Si)_3$ grown on top of a Ag buffer annealed up to 800 K. (b) Element resolved (colour) map of (a); red: Si, green: Ag, blue: Fe and yellow: C (C stems from the Pt-carbon protective layer used in the sample preparation for STEM). (For interpretation of the references to colour in this figure caption, the reader is referred to the web version of this paper.)

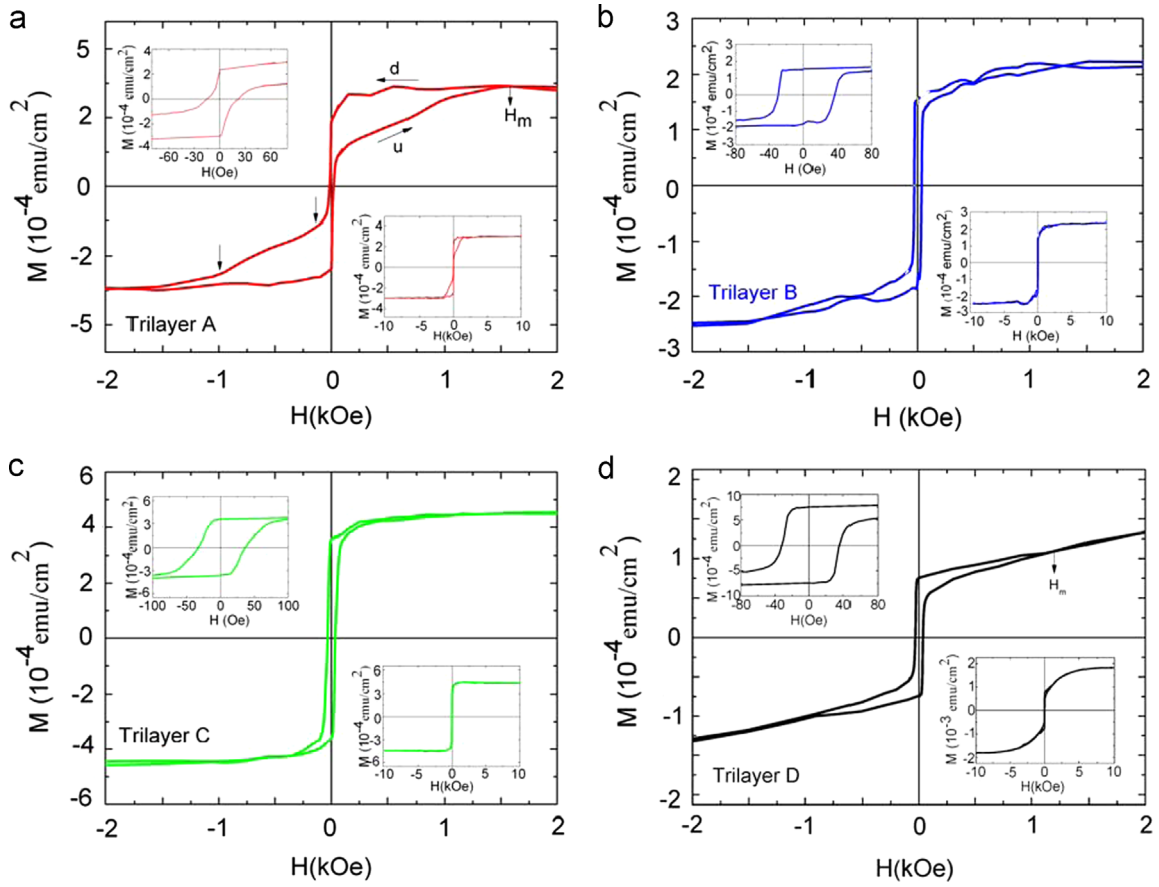

Fig. 6. The magnetization $M(H)$ per surface area unit, along the hard magnetization axis [110], at $T=5$ K, for all the multilayers in their pristine state. Insets: $M(H)$ expanded view to show the coercive field (upper left). Field range up to 10 kOe to appreciate the whole cycle to magnetization saturation (lower right). "u" and "d" in the upper left graph indicate increasing and decreasing applied field, respectively.

Table 1
Nominal Fe layer thickness, d_{Fe}, values of the coercive field, H_c, the intersection field, H_m, the saturation field, H_S, the experimental saturation magnetization, M_S, the volume fraction of non-magnetic silicides, ξ, the remanent magnetization, M_R, the M_R/M_S ratios at 5 K and the missing Fe magnetic moment expressed as equivalent thickness of Fe, Δd_{Fe}.

Sample	A	B	C	D
d_{Fe} (nm)	1.2	1.6	2.6	3.8
H_c (Oe)	20 ±2	35 ±2	36 ±2	36 ±2
H_m (Oe)	1571 ±100	–	–	1205 ±100
H_S (Oe)	1571 ±100	958 ±100	1055 ±100	8720 ±100
M_S (10^{-4} emu/cm^2)	3.07 ±0.20	2.33 ±0.20	3.90 ±0.20	14.80 ±0.20
M_S^* (10^{-4} emu/cm^2)	6.26	8.35	13.57	19.84
ξ	0.51	0.73	0.71	0.25
M_R (10^{-4} emu/cm^2)	1.99 ±0.20	1.68 ±0.20	3.26 ±0.20	5.92 ±0.20
M_R/M_S	0.65 ±0.08	0.72 ±0.11	0.84 ±0.07	0.40 ±0.01
Δd_{Fe} (nm)	0.37 ±0.04	0.69 ±0.04	1.11 ±0.04	0.58 ±0.04

direction at $H=1$ kOe, the domain structure in remanence is practically a monodomain (Fig. 7(a)). As the field applied in the negative direction increases, domains start to appear as thin threads aligned to a fixed direction in the sample plane (Fig. 7(b)) and the multilayer enters in a domain-growth regime, with domains parallel to the field (bright areas) growing at the expense of the still antiparallel aligned ones (dark areas) (Fig. 7(c, d)). In the middle of this growth regime at $H=-15.6$ Oe (Fig. 7(d)), parallel and antiparallel domains occupy similar areas, which correspond to the coercivity. The observation of two grey tones in Fig. 7(d) can be related to domains belonging to the different layers that do not reorient simultaneously [43]. At field values exceeding −18 Oe larger bright areas are formed toward a fully monodomain phase (Fig. 7(f)) attained at −81.7 Oe, where the reversible regime is reached in the MOKE loop (Fig. 7(g)).

The experimental saturation magnetization per surface unit, M_S, at 5 K is lower than the expected value for the nominal $(Fe/Si)_3$ multilayer, $M_S^*=3M_{Fe}d_{Fe}$, where $M_{Fe}=1740$ emu/cm^3 is the bulk magnetization of α-Fe, see Table 1. This decrease in M_S can be ascribed to the formation of Fe silicides at the Fe/Si interfaces during the deposition process [38], as evidenced in the TEM images and analysis in Section 3. This decrease will be quantified by

$$\xi=\frac{M_S^*-M_S}{M_S^*} \quad (1)$$

The ξ values are given in Table 1.

Zero Field Cooled (ZFC) magnetization measurements on pristine samples as a function of temperature, $M(T)$, were performed with an applied field of 1 kOe, for which the samples are magnetically saturated, except sample D. The $M(T)$ curve of the sample A is shown in Fig. 8, where some regions have been drawn in order to spotlight a different temperature dependence. From 5 K, the magnetization decreases as temperature increases (region α) because of the intrinsic magnetization thermal dependence. However, at $T_S\approx 410$ K, a sharp rise starts (region β), which has to be ascribed to phase transformation processes to a ferromagnetic phase, as it will be discussed in the next section. The following drop down to vanishing or residual magnetization (region χ) may be associated with a further phase transformation producing paramagnetic Fe silicides of the Fe–Si phase diagram, for example ϵ-FeSi [44]. Finally, after reaching 800 K, the magnetization measured during cooling to

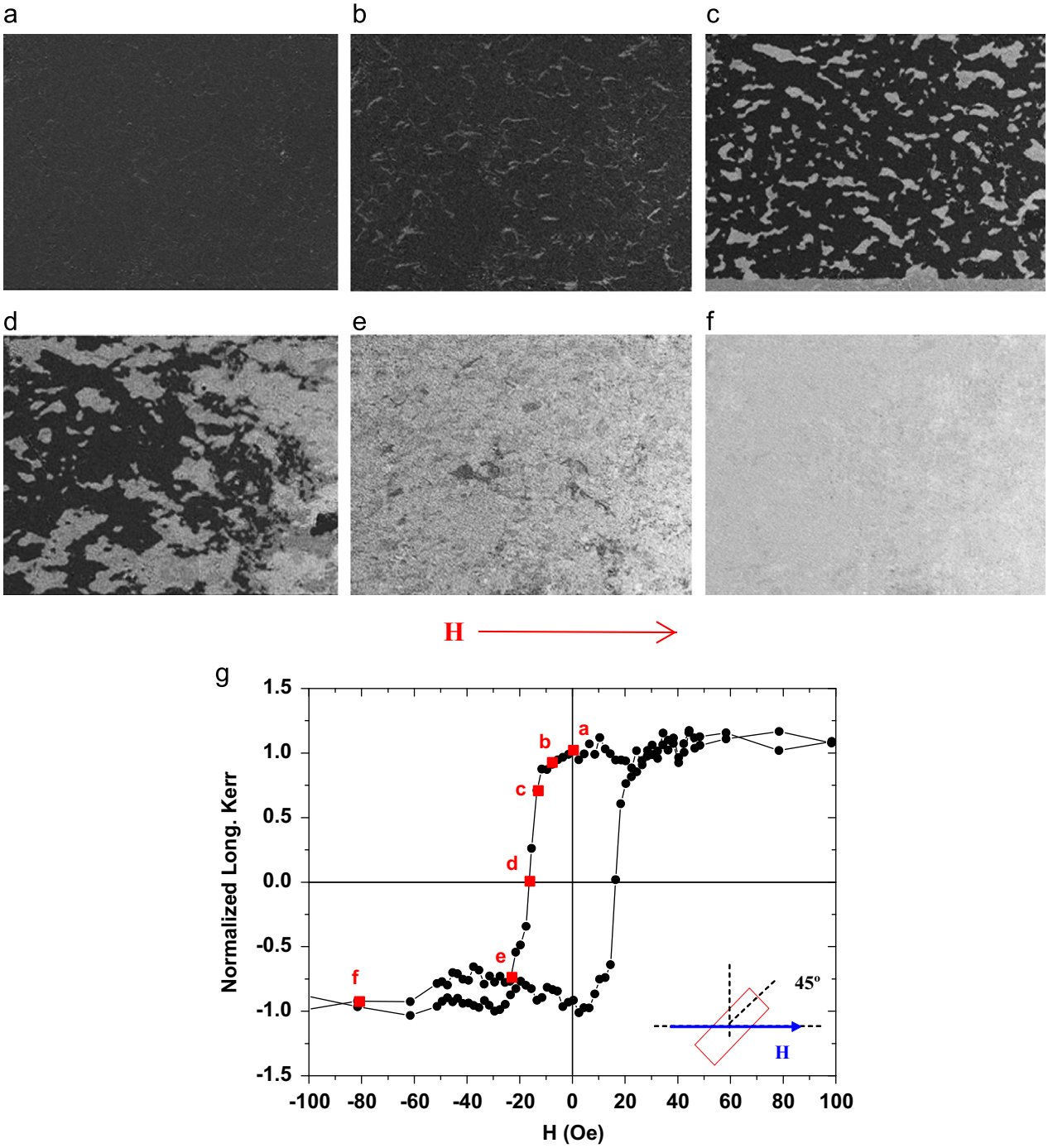

Fig. 7. (a)–(f) Field evolution of the magnetic domains in the C pristine sample. Domain images obtained at magnetic field $H=-0.7$ Oe, -7.6 Oe, -13.5 Oe, -15.6 Oe, -21.7 Oe and -81.7 Oe. (g) Hysteresis curve measured with L-MOKE at RT along Fe[100] direction; the letters indicate the corresponding images above.

room temperature (regions δ and ϵ) shows only weak reentrant magnetization. The maximum in the magnetization (M_{max}) attained at a temperature (T_{max}) and the vanishing magnetization temperature (T_f) for the different samples have been collected in Table 2.

The overall thermal behaviour of magnetization up to 800 K is similar in the four samples (Fig. 9), but a few differences may be worth pointing out. In the samples A and B, the highest value of the magnetization, attained in region β at 530 K, is very close to the magnetization at 5 K, while it is almost doubled for the case of the samples C and D. The sample D shows a remaining magnetic phase after heating up to 800 K (region ϵ) and the temperature at which the maximum in the magnetization is attained is lower. The vanishing magnetization temperature increases from sample A to D, i.e., with increasing Fe layer thickness (Table 2). These differences indicate that the phase transformations depend on the relative amount of available Fe and Si in the samples. In particular, in the sample D, with the largest amount of Fe, a ferromagnetic phase remains after annealing at high temperature.

In order to get a further insight on the process at region β, $M(T)$ at $H=1$ kOe of sample C is also shown in Fig. 10, where a sequence of thermal paths was carried out. $M(T)$ along the initial heating up to 450 K (about half way of the rise in region β) (Fig. 10, black symbols), reproduced the steep slope, starting at ≈ 410 K. However, when the temperature was lowered to 300 K, the magnetization slightly

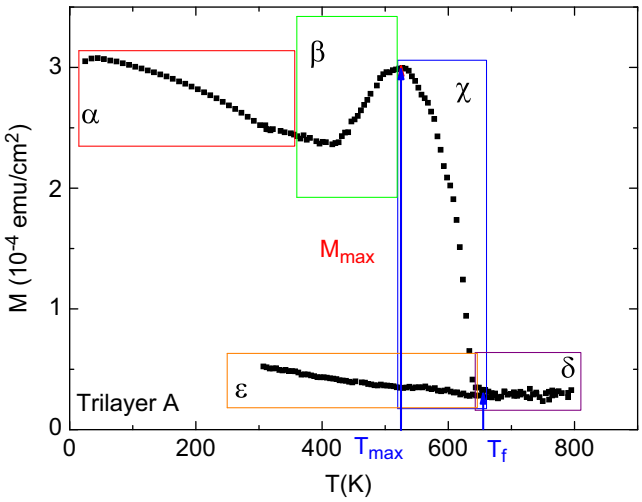

Fig. 8. The magnetization $M(T)$ per surface unit, as a function of the temperature of the pristine sample A, measured at $H=1$ kOe.

Table 2
The maximum magnetization values (M_{max}) at a temperature (T_{max}) and the vanishing magnetization temperature (T_f) for the different samples.

Sample	A	B	C	D
d_{Fe} (nm)	1.2	1.6	2.6	3.8
M_{max} (10^{-4} emu/cm^2)	3.0 ±0.2	2.5 ±0.2	7.5 ±0.2	13.5 ±0.2
T_{max} (K)	531 ±5	541 ±5	518 ±5	465 ±3
T_f (K)	635 ±5	640 ±5	690 ±5	775 ±5

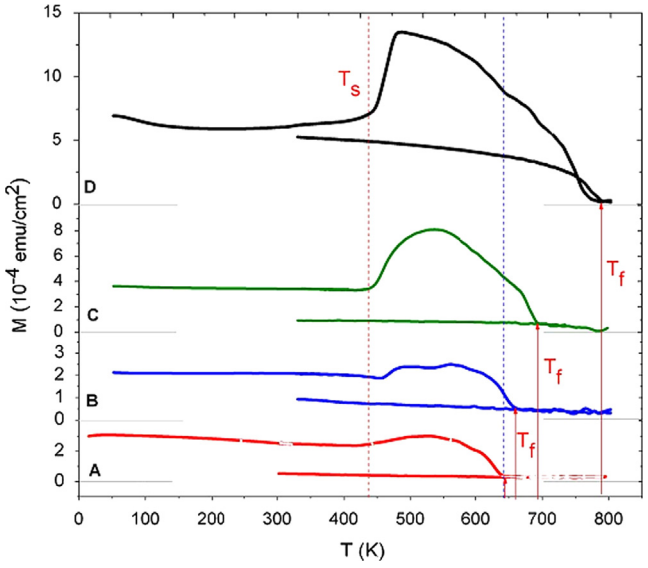

Fig. 9. The magnetization $M(T)$ per surface unit, as a function of the temperature of the different multilayers, measured at $H=1$ kOe. The vertical dashed lines indicate the rise temperature T_S and the temperature of vanishing magnetization T_f.

increased instead of coming down the slope in the 410–450 K range, which shows that an irreversible process has taken place. A second heating up to 450 K, but this time remaining at this temperature during approximately 90 min for a $M(H)$ measurement, made the magnetization increase to its maximum value (as it is indicated by the red arrow in Fig. 10). We show that the irreversible process continues until exhaustion of the reaction by depletion of the available Fe, since the final $M(T)$ from 300 K to $T_{max}=520$ K (Fig. 10, purple squares) shows no additional increase in magnetization.

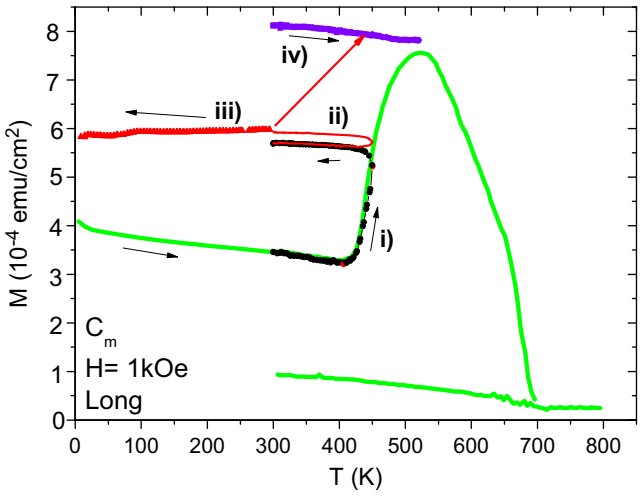

Fig. 10. The magnetization $M(T)$ per surface unit, as a function of the temperature of sample C_m (raw data), measured at $H=1$ kOe. Firstly, a continuous $M(T)$ measurement performed on a pristine sample C_m from 5 K to 800 K and cooled back to 300 K, shown in green continuous line. Secondly, $M(T)$ and $M(H)$ measurements performed on another piece of pristine sample C_m (symbols): (i) (●), a minor temperature cycle (300–450–300 K). (ii) (Red −), repetition of the previous path (300–450–300 K). (iii) (⋆), cooled back to 5 K. Then, a new repetition (300–450–300 K) with a holding time at 450 K, (iv) (■), $M(T)$ from 300 K to 520 K. (For interpretation of the references to colour in this figure caption, the reader is referred to the web version of this paper.)

5. Discussion

The HRTEM image and its FFT (Fig. 2) show that the multilayers include the epitaxially stabilized CsCl-type phase c-FeSi at the Si/Fe interfaces. Specifically, the HRTEM image (Fig. 2(a)) shows that the spacer layers are crystalline, as expected for a nominal deposited Si spacer of 1.5 nm thickness. In fact, for Si deposition larger than this value, amorphous Si is grown [23,22]. The non-magnetic c-FeSi produces a reduction in the nominal saturation magnetization of the samples by a fraction ξ (see Eq. (1) and Table 1). Alternatively, this reduction can be quantified in terms of missing Fe magnetic moment expressed as equivalent thickness of Fe [24]. Assuming that only c-FeSi is formed at the five Fe/Si interfaces (the first Fe layer is deposited on Ag), the measured saturation magnetization (in emu/cm^2) can be written as

$$M_S = (3d_{Fe} - 5\Delta d_{Fe})M_{Fe} \quad (2)$$

where Δd_{Fe} is the reduction in the nominal thickness of the Fe layer at each Fe/Si interface (missing Fe magnetic moment). Using the measured M_S values, the estimated values of Δd_{Fe} range from 0.37 to 1.1 nm/interface (see Table 1). These have to be compared with the estimated Δd_{Fe} values of 0.35–0.55 nm/interface from magnetic measurements on similar magnetic $(Fe/Si)_3$ multilayers on Si substrates [45], ≈0.32 nm/interface from CEMS spectra on (Fe 6 nm/(Si 1 nm/Fe 3.1 nm)$_3$/Si 3 nm) [46], ≈0.55 nm/interface from SAXS on (Fe 3 nm/Si 1.4 nm)$_{50}$ [24], and ≈0.43 mm/interface from the d_{Fe} dependence of MOKE on Fe/Si/Fe [25,26].

The IEC between the ferromagnetic Fe layers determines the multilayer magnetic structure in zero field [47,48]: (a) parallel or antiparallel alignment of magnetization vectors of adjacent layers for ferromagnetic (FM) or antiferromagnetic (AF) IEC, which is described by a bilinear term in the IEC energy, and (b) an orthogonal alignment of the in-plane magnetization vectors of adjacent layers, which takes place when IEC is dominated by a biquadratic exchange interaction of the relative angle between the magnetizations. The coupling strength, as estimated from the typical observed saturation fields of 1 kOe and using $M_{Fe} \times d_{Fe}$ values, which is reduced by about 1/3 due to reduced magnetization

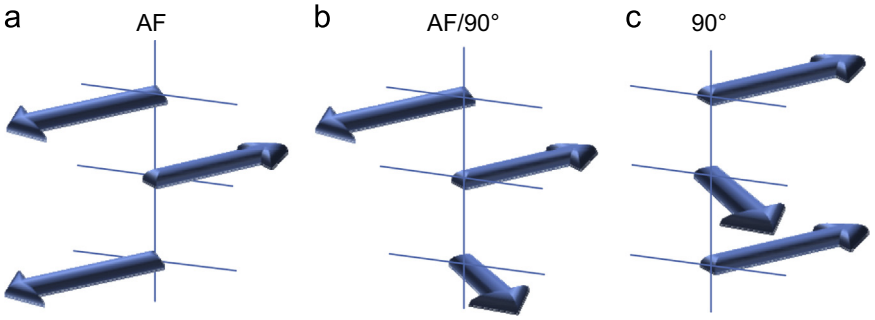

Fig. 11. Coupling configurations in remanence in a $(Fe/Si)_3$ multilayer. Thin lines indicate the hard magnetic axis.

or loss of Fe thickness due to silicide formation, has a typical value of 0.1 erg/cm^2 and is comparable to the magnetocrystalline anisotropy constant times the Fe thickness. Therefore, the anisotropy energy and the coupling energy (per unit area) are roughly of the same order of magnitude.

The multilayer magnetic structure can be derived from the remanence to saturation magnetization ratio, M_R/M_S, obtained from the hysteresis loops, as long as the magnetic layers are monodomains at remanence. The L-MOKE image at remanence (Fig. 7a) shows that this requirement is fulfilled. This can be explained by the magnetocrystalline anisotropy that tends to force the magnetization everywhere to the same easy axis orientation.

In the present system with three magnetic layers and the field applied along the hard magnetic axis, a simple model can be proposed, where the magnetization vectors of adjacent layers can be aligned either antiparallely or at a relative angle of 90° symmetrically with respect to the applied field. The parallel or ferromagnetic configuration can be discarded based on our magnetic domain image analysis. Three possible situations can be expected (Fig. 11):

(a) Three AF coupled layers at zero field (Fig. 11(a)). Assuming that each layer has equal magnetization M_L, the expected saturation magnetization is $M_S = 3M_L$ and at zero applied field the remanence component along the hard axis direction is $M_R = (2-1)(1/\sqrt{2})M_L$, and $M_R/M_S = 0.24$.
(b) The first two deposited layers are coupled at 90° while the third one is antiparallel to its neighbouring magnetic layer (Fig. 11(b)). Then, $M_R = (\sqrt{2}-\sqrt{2}/2)M_L$ and $M_R/M_S = 0.24$. Note that this configuration requires that the IEC through the two spacers layers is different. We may denote this configuration 90°-AF.
(c) The three layers are coupled at 90° (Fig. 11(c)), then $M_R = (\sqrt{2}+\sqrt{2}/2)M_L$ and $M_R/M_S = \sqrt{2}/2 = 0.71$.

For samples A–C ($d_{Fe} = 1.2$–2.6 nm) $M_R/M_S \approx 0.7$ is similar to previous results for $n=2$ and 4 [34] and it is consistent with a 90° coupling. In contrast, sample D, with the largest Fe layer thickness ($d_{Fe} = 3.8$ nm), shows $M_R/M_S = 0.40$ with a very high H_s, which indicates a superposition of 90° and AF components in the alignment of the layer magnetization vectors. Additionally, the L-MOKE measurements in the magnetic field mid-range show a micrometric magnetic domains structure (Fig. 7) similar to that found in AF coupled Co/Cu [49], or 90° coupled Fe/Cr/Fe [43] multilayers, and discard the FM (three parallel magnetization vectors) coupling.

Since in all the present samples the Si spacer layers have the same thickness, the difference in the hysteresis loop shapes and M_R/M_S ratios (Fig. 12, Table 1) must be ascribed to the variation in the Fe layer thickness. These $[Fe(d_{Fe})/Si(1.5\text{ nm})]_3$ multilayers constitute a particular case of $(Fe/Si)_n$ with small and *odd* n number. As shown in [34], for the $(Fe(3\text{ nm})/Si(1.4\text{ nm}))_n$ multilayers with even n and layer thickness very close to the present case, M_R/M_S decreases fast with increasing n. Although the AF coupling is observed for large n values [22,33,34], MOKE experiments on both sides of the multilayers have shown that, for a given spacer thickness, the magnetic layers close to the substrate couple at 90° while the next layers couple antiferromagnetically. Then, in the case of very few bilayers the 90° coupling of the first layers is expected to dominate, while the coupling type should change to AF as the number of Fe/Si bilayers increases [34]. However, the present $(Fe/Si)_3$ multilayers give evidence that the IEC is 90°-coupling for low Fe layers thickness and evolves to include an AF component as d_{Fe} increases. In fact, a strong AF coupling across Si spacers has previously been observed in 5 nm Fe/Si(t)/5 nm Fe trilayers with $t \leq 2.2$ nm [36,37], i.e., in samples with thicker Fe layers than in the present work.

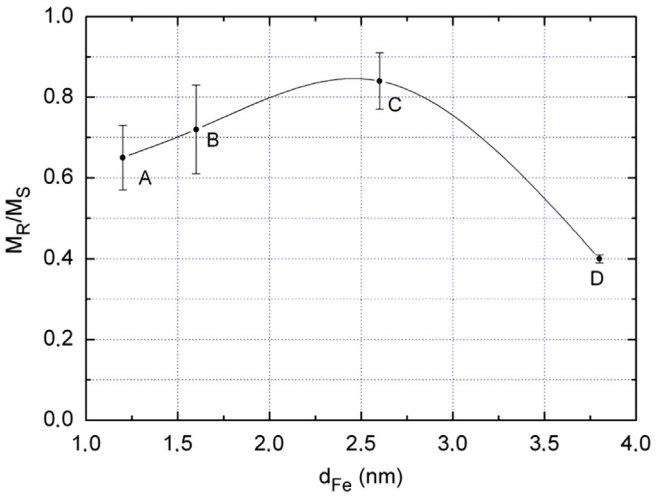

Fig. 12. Dependence of the M_R/M_S ratio with the deposited Fe layer nominal thickness. The letters correspond to the designations of the samples.

The zero field cooled $M(T)$ curves of the as-prepared, pristine samples grown on the GaAs/Fe/Ag substrate measured at $H=$ 1 kOe, decreases continuously up to 410 K (region α, Fig. 8), as expected because of the intrinsic decrease of the magnetization of Fe for increasing temperature. However, for $T > 410$ K, $M(T)$ (region β, Fig. 8), we observe a rounded anomaly with a maximum at T_{max}. This feature can be explained as follows: t|he Fe and Si atoms diffuse and react at the interlayers, already upon deposition at room temperature, producing c-FeSi. Then, at temperatures higher than 410 K, the diffusion/reaction process is reactivated, modifying the interface and the spacer layers' compositions. The diffusion coefficient (D_0) of Fe in Si and Si in Fe is so different ($D_0 = 0.0062$ cm^2/s and $D_0 = 0.7$ cm^2/s, respectively) that it can be foreseen that Fe stemming from the α-Fe layer diffuses towards the Si rich side of the interface [50]. Since the diffusion process always takes place in the direction of the concentration gradient of

components, that is, perpendicular to the layer plane, the composition of the interlayer depends on the depth. The reaction to new compositions takes place as the diffused atoms reach the components of the as-prepared state, namely paramagnetic c-FeSi. Since we observe a net increase of the saturation magnetization in the anomaly for increasing temperature up to T_{max}, it is evident that the new compositions need to be a ferromagnetic Fe(Si) solid solution. The as-deposited structure transforms progressively into a new stack containing the ferromagnetic Fe(Si) solid solution with a higher Fe content near the remaining α-Fe. In short, the sharp rise in the magnetization at T higher than 410 K can only be understood if the paramagnetic c-FeSi phase transforms gradually into a ferromagnetic Fe(Si) phase.

At temperatures above T_{max}, the decrease in magnetization can be produced by the approach to the Curie temperature of the magnetic phase and/or by phase transformation to a paramagnetic phase. Since T_C for the magnetic $Fe_{1-x}Si_x$ ($x \approx 0.25$) is 860 K [51], well above T_f, phase transformation is expected to be the major process. While samples A,B and C show a smooth decrease in $M(T)$ down to zero at T_f, sample D displays two additional features: two shoulders in the temperature range $T_{max} < T < T_f$, and a non-vanishing magnetization at T_f (Fig. 9). This behaviour is similar to that shown in the transformation of Fe_3Si deposited on a Si substrate into Fe_3Si with increased disorder and the appearance of ϵ-FeSi, as observed by X-ray diffraction upon annealing up to 850 K and subsequent cooling [52]. The total Si and Fe deposited on the substrate in the case of the sample D amounts to an overall composition of 40% at. Si. Then, if all Fe and Si have reacted when the sample is heated up to 800 K, the subsequent room temperature microstructure is expected to be composed of two phases, according to the Fe–Si phase diagram [44]: ϵ-FeSi (paramagnetic) and $Fe_{1-x}Si_x$ with $x \approx 0.27$, whose $T_C = 800$ K [51], in agreement with $T_f = 775$ K, the vanishing temperature encountered in sample D (Table 2). In contrast, sample C shows an overall composition of 50% at. Si., or a final ϵ-FeSi phase; obviously this percentage is even larger for samples A and B and, in any case, the final equilibrium phases would be paramagnetic.

In the $(Fe/Si)_3$ heterostructures with the same Si spacer and Fe layer thicknesses [38] but grown on Si(100) and Si(111) substrates with a silicon oxide buffer layer no anomaly is observed; in fact, $M(T)$ decreases monotonously till complete vanishing at temperature T_f. Therefore, no ferromagnetic phase is produced in that case, but rather a progressive transformation towards the paramagnetic final phases takes place. The difference in behaviour is, consequently, caused by the two different types of preparation methods which give rise to different relative amounts of the Fe silicides at the interfaces in the as-prepared samples. Therefore, the final phases obtained at the highest temperature (T_f) are controlled by the amount of available Fe and the starting point in the Fe–Si phase diagram, while the dynamics of this process is controlled by the geometric distribution of Si in the heterostructures. The reactions involved are irreversible and, consequently, the thermomagnetic behaviour is also irreversible above 410 K.

6. Conclusions

Well-defined $(Fe/Si)_3$ multilayers have been obtained on a substrate formed by a buffer layer of Fe/Ag deposited on GaAs (001) by thermal evaporation in an ultrahigh vacuum system. HRTEM images show that Fe–Si atomic migration and a subsequent chemical reaction process occur during the sample preparation, and during the annealing of the samples. Chemical maps evidence the presence of Fe in the Si layers and hardly any quantity of Si in the Fe layers in the pristine samples. STEM measurements show that most of the iron is in the bcc Fe phase, while the rest has reacted with Si, forming silicides at the interfaces. Moreover, the periodicities of the Fast Fourier Transform (FTT) of the HRTEM image do not match the conventional Si structure, but the epitaxially stabilized c-FeSi phase. After annealing up to 800 K the multilayer system is transformed progressively into a mixture of all the components with Fe–Si grains inside the original buffer of Ag.

We have shown that the reduced and odd number of Fe films, $n=3$, plays a role for the magnetic properties of these films. The hysteresis loops at 5 K yield values of the M_R/M_S ratios and saturation fields, which indicate a 90° coupling in all samples, except in sample D, where AF inter-layer coupling is proposed to co-exist with 90°-coupling. These M_R/M_S values follow the dependence on the number of (Fe/Si) bilayers as observed by Reference [34] on $(3\text{ nm Fe}/1.1\text{ nm Si})_n$ multilayers with even n, except for the sample with the largest Fe thickness. The antiferromagnetic IEC strengths observed in this work are of the order of 0.1 erg/cm^2 and thus almost one order of magnitude lower than those reported previously for epitaxial Fe/Si/Fe(001) trilayers [36,37]. The optimized sample properties of Fe/Si/Fe(001) multilayers for strongest AF coupling remain an open question, just as the detailed understanding of the interlayer exchange coupling across Si spacer layers.

The $M(T)$ curve on the pristine samples shows an irreversible thermal process, with a rise in the magnetization in all compounds at a common temperature of about 410 K. From this temperature up to T_{max}, the thermal irreversibility is associated with a modification of the spacer and multilayer constitution upon heating due to atomic diffusion and chemical reaction of Fe with Si. The paramagnetic silicide formed at the deposition stage of sample preparation is transformed into a ferromagnetic Fe silicide phase. These transformation processes evolve with time, with the increasing magnetization as time elapses at that fixed temperature.

This peculiar $M(T)$ irreversible process is not present in the previously studied $(Fe/Si)_3$ multilayers [38]. The difference between both types of samples resides in the fact that the present samples are deposited on GaAs/Fe/Ag(001), while the others are deposited on Si/SiO_2. The Fe/Ag buffer in the present samples allows not only an epitaxial growth of the multilayer, but also limits the possibility of the Fe to react exclusively with the Si in the spacers. In contrast, in the samples deposited on Si/SiO_2, the Fe can also react with Si stemming from the substrate, which allows the formation of Fe silicides phases with a higher Si content. Therefore, the heating process in the two types of samples may have very different effects on the subtle changes in the Si spacer layer due to diffusion and chemical reaction, stress relaxation and defect annihilation that modify the IEC, and is put in evidence by the change of phases which are present in the spacers after heating the pristine, epitaxially grown samples.

From temperature T_{max} up to T_f (Table 2), an irreversible decrease in the magnetization of the $(Fe/Si)_3$ multilayer occurs corresponding to the transformation into nonmagnetic silicides. The temperature at which the process is completed (T_f) depends on the kinetics of the reaction and the available amount of each atomic species. Sample D is the only one where some magnetic phase remains, besides the paramagnetic FeSi phase.

To conclude, the $(Fe/Si)_n$ multilayers conserve their integrity just till $T \approx 410$ K, above which chemical reactions, which we have shown here to critically depend on the substrate material, modify their morphology.

Acknowledgements

The financial support of the Spanish MINECO MAT2011-23791, FIS2008-06249, the President of Russia Grant (NSh-1044.2012.2),

RFFI Grant 13-02-01265, 14-0290404, Aragonese DGA-IMANA E34 (cofunded by Fondo Social Europeo) and that received from the European Union FEDER funds is acknowledged. L.B.R. acknowledges the Spanish MINECO FPU 2010 grant. Authors would like to acknowledge the use of Servicio General de Apoyo a la Investigación-SAI, Universidad de Zaragoza.

References

[1] M.N. Baibich, J.M. Broto, A. Fert, F.N. Van Dau, F. Petroff, P. Etienne, G. Creuzet, A. Friederich, J. Chazelas, Phys. Rev. Lett. 61 (1988) 2472–2475.
[2] R.E. Camley, R.L. Stamps, J. Phys.: Condens. Matter 5 (1993) 3727.
[3] J. Sesé, J. Bartolomé, C. Rillo, Rev. Sci. Instrum. 78 (2007) 04610.
[4] G.S. Patrin, N.V. Volkov, V.P. Kononov, JETP Lett. 68 (1998) 307.
[5] G.S. Patrin, S.G. Ovchinnikov, D.A. Velikanov, V.P. Kononov, Phys. Solid State 43 (2001) 1712.
[6] G.S. Patrin, N.V. Volkov, S.G. Ovchinnikov, E.V. Eremin, M.A. Panova, S.N. Varnakov, JETP Lett. 80 (2004) 491.
[7] G.J. Strijkers, J.T. Kohlhepp, H.J.M. Swagten, W.J.M. de Jonge, Phys. Rev. Lett. 84 (2000) 1812–1815.
[8] R.R. Gareev, D.E. Bürgler, M. Buchmeier, D. Olligs, R. Schreiber, P. Grünberg, Phys. Rev. Lett. 87 (2001) 157202.
[9] D.E. Bürgler, M. Buchmeier, S. Cramm, S. Eisebitt, R.R. Gareev, P. Grünberg, C.L. Jia, L.L. Pohlmann, R. Schreiber, M. Siegel, Y.L. Qin, A. Zimina, J. Phys.: Condens. Matter 15 (2003) S443–S450.
[10] S. Datta, B. Das, Appl. Phys. Lett. 56 (1990) 655.
[11] S.A. Wolf, D.D. Awschalom, R.A. Buhrman, J.M. Daughton, S.V. Molnar, M.L. Roukes, A.Y. Chtchelkanova, D. Treger, Science 294 (2001) 1488.
[12] T. Yoshitake, Y. Inokuchi, A. Yuri, K. Nagayama, Appl. Phys. Lett. 88 (2006) 182104.
[13] M. Shaban, K. Nakashima, W. Yokoyama, T. Yoshitake, Jpn. J. Appl. Phys. 46 (2007) L667.
[14] M. Milosavljević, G. Shao, N. Bibić, C.N. McKinty, C. Jeynes, K.P. Homewood, Appl. Phys. Lett. 79 (2001) 1438.
[15] T. Yoshitake, M. Yatabe, M. Itakura, N. Kuwano, Y. Tomokiyo, K. Nagayama, Appl. Phys. Lett. 83 (2003) 3057.
[16] K. Takarabe, H. Doi, Y. Mori, K. Fukui, Y. Shim, N. Yamamoto, T. Yoshitake, K. Nagayama, Appl. Phys. Lett. 88 (2006) 061911.
[17] J.E. Mattson, E.E. Fullerton, S. Kumar, S.R. Lee, C.H. Sowers, M. Grimsditch, S.D. Bader, J. Appl. Phys. 75 (1994) 6169.
[18] J.M. Gallego, J.M. García, J. Alvarez, R. Miranda, Phys. Rev. B 46 (1992) 13339–13344.
[19] T. Yoshitake, D. Nakagauchi, T. Ogawa, M. Itakura, N. Kuwano, Y. Tomokiyo, T. Kajiwara, K. Nagayama, Appl. Phys. Lett. 86 (2005) 262505.
[20] M. Gomoyunova, D. Malygin, I. Pronin, A. Voronchikhin, D. Vyalikh, S. Molodtsov, Surf. Sci. 601 (2007) 5069.
[21] I.I. Pronin, M.V. Gomoyunova, D.E. Malygin, D.V. Vyalikh, Y.S. Dedkov, S.L. Molodtsov, J. Appl. Phys. 104 (2008) 104914–104923.
[22] E.E. Fullerton, J. Mattson, S. Lee, C. Sowers, Y. Huang, G. Felcher, S. Bader, F. Parker, J. Magn. Magn. Mat. 117 (1992) L301–L306.
[23] K. Inomata, K. Yusu, Y. Saito, Phys. Rev. Lett. 74 (1995) 1863–1866.
[24] A. Chaiken, R.P. Michel, M.A. Wall, Phys. Rev. B 53 (1996) 5518–5529.
[25] J.J. de Vries, J. Kohlhepp, F.J.A. den Broeder, R. Coehoorn, R. Jungblut, A. Reinders, W.J.M. de Jonge, Phys. Rev. Lett. 78 (1997) 3023–3026.
[26] J. de Vries, J. Kohlhepp, F. den Broeder, P. Verhaegh, R. Jungblut, A. Reinders, W. de Jonge, J. Magn. Magn. Mater. 165 (1997) 435–438.
[27] Y. Shin, D.A. Tuan, Y. Hwang, T.V. Cuong, S. Cho, J. Appl. Phys. 113 (2013) 17C306.
[28] G. Binasch, P. Grünberg, F. Saurenbach, W. Zinn, Phys. Rev. B 39 (1989) 4828–4830.
[29] S. Wolf, L. Jiwei, M.R. Stan, E. Chen, D.M. Treger, Proc. IEEE 98 (2010) 2155–2168.
[30] S. Toscano, B. Briner, H. Hopster, M. Landolt, J. Magn. Magn. Mater. 114 (1992) L6–L10.
[31] E.E. Fullerton, J.E. Mattson, S.R. Lee, C.H. Sowers, Y.Y. Huang, G. Felcher, S.D. Bader, F.T. Parker, J. Appl. Phys. 73 (1992) 6335–6337.
[32] Y. Endo, O. Kitakami, Y. Shimada, IEEE Trans. Mag. 34 (1998) 906–908.
[33] Y. Endo, O. Kitakami, Y. Shimada, Phys. Rev. B 59 (1999) 4279–4286.
[34] J. Kohlhepp, F. den Broeder, M. Valkier, A. van der Graaf, J. Magn. Magn. Mater. 165 (1997) 431–434.
[35] P. Bruno, Phys. Rev. B 52 (1995) 411–439.
[36] R.R. Gareev, D.E. Bürgler, M. Buchmeier, R. Schreiber, P. Grünberg, J. Magn. Magn. Mater. 240 (2002) 235–237.
[37] R.R. Gareev, D.E. Bürgler, M. Buchmeier, R. Schreiber, P. Grünberg, Appl. Phys. Lett. 81 (2002) 1264.
[38] S.N. Varnakov, S.V. Komogortsev, S.G. Ovchinikov, J. Bartolomé, J. Sesé, J. Appl. Phys. 104 (2008) 094703.
[39] D. Bürgler, C. Schmidt, J. Wolf, T. Schaub, H.-J. Guntherodt, Surf. Sci. 366 (1996) 295.
[40] Z.Q. Qiu, J. Pearson, S.D. Bader, Phys. Rev. Lett. 70 (1993) 1006–1009.
[41] M. Buchmeier, B.K. Kuanr, R.R. Gareev, D.E. Bürgler, P. Grünberg, Phys. Rev. B 67 (2003) 184404.
[42] L.J. Swartzendruber, Bull. Alloy Phase Diagr. 5 (1984).
[43] M. Rührig, R. Schäfer, A. Hubert, R. Mosler, J.A. Wolf, S. Demokritov, P. Grünberg, Phys. Status Solidi (a) 125 (1991) 635.
[44] U. Starke, J. Schardt, W. Weiss, W. Meier, C. Polop, P.L. de Andres, K. Heinz, Europhys. Lett. 56 (2001) 822.
[45] S.N. Varnakov, J. Bartolomé, J. Sesé, S.G. Ovchinnikov, S.V. Komogortsev, A.S. Parshin, G.V. Bondarenko, Phys. Solid State 49 (2007) 1470–1475.
[46] G.J. Strijkers, J.T. Kohlhepp, H.J.M. Swagten, W.J.M.d. Jonge, Phys. Rev. B 60 (1999) 9583–9587.
[47] E.E. Fullerton, S.D. Bader, Phys. Rev. B 53 (1996) 5112–5115.
[48] S.O. Demokritov, J. Phys. D, Appl. Phys. 31 (1998) 925–941.
[49] J.A. Borchers, J.A. Dura, J. Unguris, D. Tulchinsky, M.H. Kelley, C.F. Majkrzak, S.Y. Hsu, R. Loloee, W.P. Pratt, J. Bass, Phys. Rev. Lett. 82 (1999) 2796–2799.
[50] C.J. Le Thanh Vinh, J. Derrien, Phys. Rev. B 46 (1992) 15946–15954.
[51] L.K. Varga, F. Mazaleyrat, J. Kovac, J.M. Greneche, J. Phys.: Condens. Matter 14 (2002) 1985.
[52] K. Takeda, T. Yoshitake, Y. Sakamoto, D. Hara, M. Itakura, N. Kuwano, K. Nagayama, Int. J. Mod. Phys. B 23 (2009) 3543.